# Experimental Characterization of Geometry-Based Channel Models in Suburban Microcells

Claude Oestges and Natalia Dementieva
ICTEAM
Université catholique de Louvain
Louvain-la-Neuve, BELGIUM

Evgenii Vinogradov
ESAT-TELEMIC
KU Leuven
Leuven, BELGIUM

*Abstract* — **This paper evaluates MIMO radio channel measurements at 3.8 GHz, conducted in various urban microcellular environments in the city of Louvain-la-Neuve, Belgium. Large-scale parameters, such as shadow fading, delay and angular spreads as well as dense multipath power are extracted and compared with values provided by existing models. A joint specular-dense multipath cluster-based model is then parametrized from the experimental data, detailing cluster spread and correlation properties.**

*Index Terms*—**Channel modeling, channel sounding, GBSCM.**

## I. Introduction

The unprecedented growth of mobile data traffic will lead to significant modifications in the architecture of wireless networks. The optimal design and implementation of future radio technologies require accurate channel models that reproduce the real-world behavior of radio channels in many use cases.

However, existing advanced models, such as the WINNER and COST families of models [1-3], still lack several features such 3-D propagation, as well as parameter tables for many interesting scenarios. In addition, the validation of such models against measurements in relevant scenarios is often an open issue. As part of the effort to parametrize and validate the COST 2100 model, this paper

- analyzes the properties of large-scale parameters (LSPs), such as shadow fading, delay and angular spreads and dense multipath components (DMC) in two microcell scenarios, and compares the obtained values with those provided by the aforementioned standard models,
- proposes a cluster-based parameterization of the COST 2100 channel model based on the recoded data; this is the first time that parameters for the COST 2100 model are provided for microcellular environments.

The paper is organized as follows: Section II is dedicated to the measurement campaign, while Section II details the LSP analysis, including their cross-correlation properties. Finally, Section IV details the cluster-based model.

## II. Measurement Campaigns

### A. Microcellular Scenarios

Two 8 × 8 MIMO measurement runs were performed in a microcell-lie environment in the city of Louvain-la-Neuve. The base station (BS) was located atop a high building, at a height of 18 m and consisted in a 4 dual-polarized planar array with orthogonal slanted polarizations and a 3-dB beamwidth of 95°. At the mobile station (MS), a uniform circular array of 8 vertically polarized dipoles was used. All dipoles were spaces by approximately 4 cm. The antenna array was placed on a moving trolley at a height of 2 m.

In the first scenario (denoted as “Parking”, or simply *P*), the MS was moved at pedestrian speed (roughly 0.8 m/s) on the parking lot, consisting in a large open space area with some cars and trees on its perimeter. Most of the route was in line-of-sight (LOS) with respect to the BS, with occasional obstructed LOS (OLOS) caused by trees. In the second measurement campaign (denoted as “Sainte-Barbe”, or *SB*), the MT was moved at pedestrian speed (roughly 0.8 m/s) long streets between various buildings with 4-5 floors, resulting in heavy non-LOS (NLOS) conditions for some parts of the route. Fig. 1 illustrates both routes as obtained from GPS data. The route lengths are approximatively 170 and 230 meters for the parking and Sainte-Barbe, respectively. The distance from the BS to the MS never exceeded 300 meters.

### B. Sounding Setup

The UCL-ULB Elektrobit channel sounder was used in a MIMO 8 × 8 configuration. The sounder is based on the switched array principle and the parameters chosen for the experimental campaigns are given in Table I. The cycle rate corresponds to the inverse acquisition time of one MIMO matrix. Given the

terminal's speed, this corresponds to one MIMO matrix every 2.7 cm.

In the post-processing step, all MIMO channels were converted to double-directional channel impulse responses (CIRs), based on the Space-Alternating Generalized Expectation-Maximization algorithm, usually known as SAGE (the so-called ISIS™ SAGE implementation of the Elektrobit channel sounder has been used in this work). This algorithm fully de-embeds the 3-D antenna patterns at both sides. For each route, a maximum of 30 paths were resolved; each path was characterized by its delay, azimuth at the BS, azimuth and elevation at the MS and polarized scattering matrix.

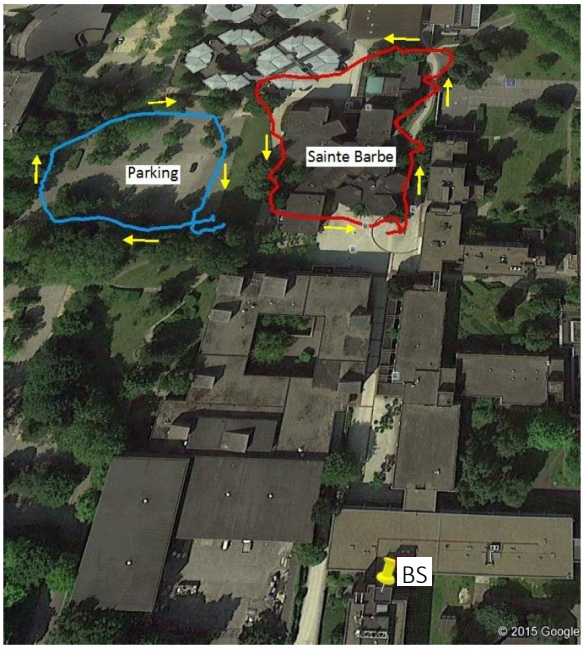



Fig 1. Measurement routes and BS location.

TABLE I. MEASUREMENT SETUP

| Parameter | Value |
|---|---|
| Center frequency | 3.8 GHz |
| Bandwidth | 200 MHz |
| Samples per chip | 4 |
| Cycle rate | 30.2 Hz |
| Transmit Power | 23 dBm |
| Code length | 5.11 µs |

## III. ESTIMATION OF LARGE-SCALE PARAMETERS

### *A. Path-Loss and Shadow Fading*

A sliding window equal to 40 wavelengths was used to separate the average received power and from the small-scale fading. The path-loss exponents were estimated as 2.2 and 3.9 for both *P* and *SB* scenarios, respectively: these values match well with the LOS and NLOS conditions observed for both environments. The shadow fading component was found to be lognormal with a standard deviation of 1.31 dB in the parking area and 3.37/0.59 dB in the *SB* scenario in NLOS/LOS respectively.

### *B. Delay- and Direction-Spreads*

The Root-Mean-Square (RMS) delay-spread is estimated from both the full power-delay profiles, and those reconstructed based on the resolved paths only (see Section III.C for the discussion on the residual power). Results are given in Table II in terms of mean standard deviation (std) values of the RMS delay-spread. For both scenarios, the measured values are quite close the values of 36 and 76 ns predicted by WINNER II B1 model, respectively for LOS and NLOS scenarios. However, by contrast to this model, the delay-spread is only weakly correlated with the shadow fading.

TABLE II. MEAN (STD) OF RMS DELAY-SPREADS, [NS]

| | SAGE CIR | Full CIR |
|---|---|---|
| **Parking** | 36 (16) | 78 (19) |
| ***SB* - LOS** | 51 (37) | 83 (58) |
| ***SB* - NLOS** | 54 (39) | 96 (35) |

RMS direction-spreads are estimated from the SAGE resolved paths. The average values at each location are also illustrated in Figure 2 and their statistics are given in Table III for azimuth-spreads (AS) at both sides and elevation-spread (ES) at MS.

TABLE III. MEAN (STD) OF ANGLE-SPREADS, [DEGREES]

| | AS at BS | AS at MS | ES at MS |
|---|---|---|---|
| **Parking** | 13 (6) | 38 (11) | 31 (9) |
| ***SB* - LOS** | 24 (10) | 35 (13) | 32 (11) |
| ***SB* - NLOS** | 25 (11) | 41 (12) | 31 (10) |

When compared with standardized models, one can observe that the BS azimuth-spread for the NLOS *SB* scenario agrees perfectly with the prediction of 3GPP UMi model. For the LOS *SB* case, there is a large difference between our result and both 3GPP (16°) and WINNER II B1 model (2.5°), but this might be caused by the fact that some LOS locations are actually OLOS. It must be noted that the QuaDRiGa campaign reported azimuth-spreads at the BS between 7 and 22 degrees in NLOS conditions, which are in line with the values of Table III.

Looking at the azimuth-spread at the MS side, the results obtained from measurements (Table III) are much closer to the WINNER II B1 model than to the 3GPP UMi case. Our values also tend to be very close to those reported by the QuaDRiGa campaign [4].

We also found a correlation around 0.45 between AS and ES at the MS, unlike 3GPP UMi, which recommend only 0.2. In all cases, the correlation between all angle-spreads was always below 0.5.

Finally, by contrast to both 3GPP and WINNER II models, as well as results in [5], we did not find any strong correlation between RMS delay- and directional-spreads. Note that this was also observed in [6].

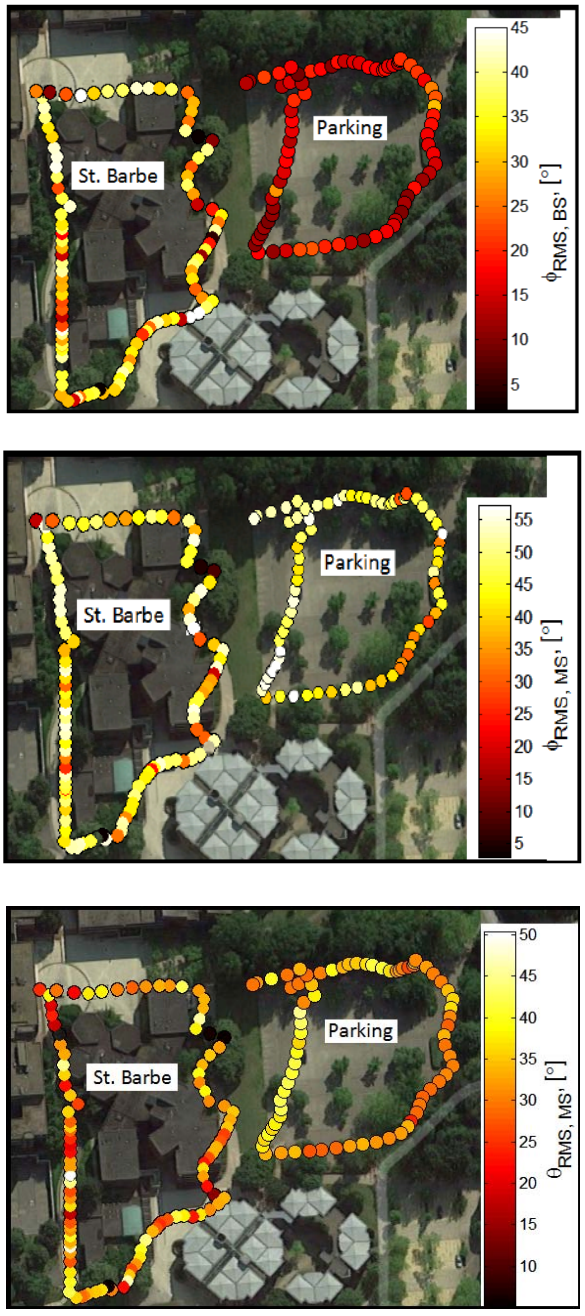



Fig 2. BS (top) and MS (middle) azimuth-spreads and MS elevation-spreads for both routes.

### C. Dense Multipaths

Specular paths estimated by the SAGE algorithm do not account for the total power of the CIRs. The residual [3] is usually known as the dense multipath components (DMCs) and is estimated as the difference between the full CIR and the reconstructed CIR based on specular paths (i.e. the SAGE discrete paths are filtered over the channel sounder bandwidth). Fig. 3 illustrates this estimation at a particular position.

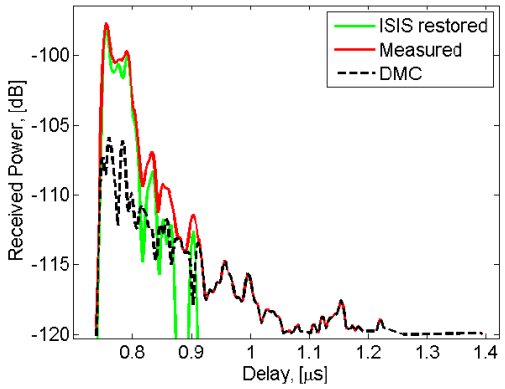



Fig. 3. Estimation of DMC at one particular position (parking route).

In this particular case, dense multipaths account for 25 % of the total power (i.e. SAGE extracts 75% of the power). On average, for both routes, the average specular power is 58 %, although there is a correlation between the shadow fading value and the specular power: in the LOS (or obstructed LOS) segments, the average recovered power reaches 90%, but values as low as 20% can be reached in deep NLOS segments.

## IV. Geometry-Based Model Parametrization

### A. Cluster Extraction

Based on the set of discrete multipaths extracted by the SAGE algorithm, a K-Power Means (KPM) clustering algorithm has been used, relying on the Kim-Parks index to estimate the optimal number of clusters.

Intuitively, the KPM algorithm clusters paths in a multi-dimensional space (delay and angles), also weighting each path by its power [7]. The resulting number of clusters (illustrated in Fig. 4 for the *SB* route) varies from 3 to 14 on the parking route (mean of 5.2) and from 2 to 14 on the *SB* route (mean values of 5.4 and 5.1 for NLOS and LOS, respectively).

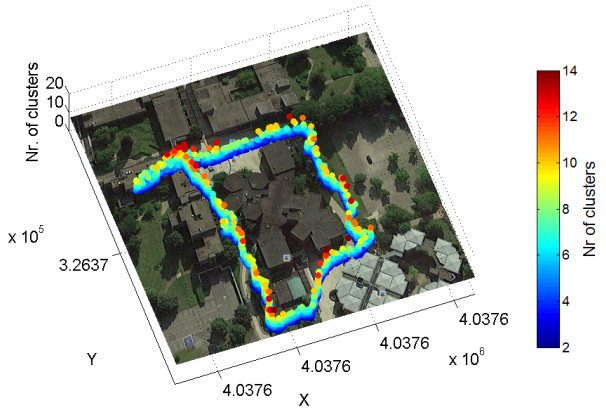


Fig. 4. Estimated number of clusters per data point on the *SB* route.

The number of paths per cluster fluctuates between 1 and 20 for the *SB* NLOS segments. In LOS conditions, clusters contain up to 16 waves. For the parking route, the number of specular components per cluster varies between 1 and 24. Singleton clusters with just one MPC visually correspond to a strong specular reflection with very high power. The average number of paths per cluster is equal to 3.6 and 3.8 for the *SB* LOS and NLOS segments, respectively, to 4.5 on the parking route. Fig. 5 illustrates the clustering results for a given location along the parking route.

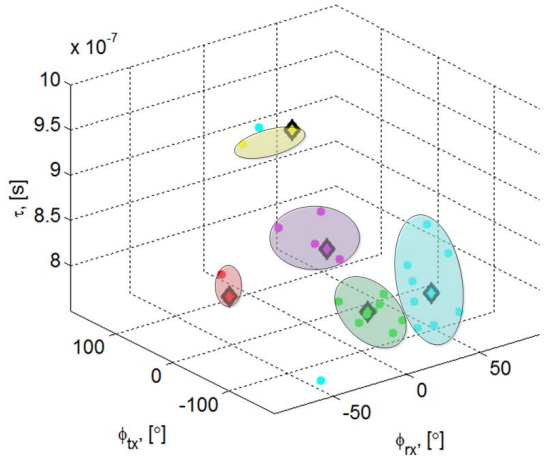



Fig. 5. Clustering example on the parking route (the centers of the cluster centroids are drawn as diamonds).

## *B. Cluster Parameterization for Specular Paths Only*

Each cluster is then characterized by its power, average delay and average angle of departure and arrival, as well as by spread values.

*1) Cluster Power:* The cluster power in [dB] appears to linearly decay with the mean cluster delay, corresponding to the delay of its centroid. The decay factor equals 23 and 33 dB/µs, for the parking and the *SB* routes respectively.

*2) Cluster Spreads:* As shown in Table IV, the lowest values of cluster delay and azimuth-spreads (CDS and CAS) are observed in LOS conditions. The azimuth-spreads at the MS for both routes in NLOS segments are very close (around 11 degrees). The azimuth-spread at the BS is larger at the SB, but is considerably lower the MS values, which is expected.

TABLE IV. MEAN (STD) OF CLUSTER SPREADS

| | **CDS [ns]** | **CAS at BS [deg.]** | **CAS at MS [deg.]** |
|---|---|---|---|
| **Parking** | 11.3 (2.6) | 5.4 (3.3) | 10.1 (3.3) |
| ***SB* - LOS** | 4.7 (2.3) | 5.3 (3.5) | 8.9 (3.8) |
| ***SB* - NLOS** | 8.8 (2.5) | 6.5 (3.8) | 10.1 (3.9) |

As a comparison, the 3GPP 3D-UMi model considers an average number of clusters of 12 and 19 in LOS/NLOS respectively, average CAS of 3 and 10 degrees (LOS/NLOS) at the BS and of 17 and 22 degrees (LOS/NLOS) at the MS. The BS values are in the same as those observed in our data, but the MS values are somewhat larger than our own observations. The same conclusion could be made with the COST 273 model, which tends to provide much larger cluster spreads. Further discussion on this discrepancy is provided in Section IV.C, where DMCs are also accounted for in the cluster parameterization. Comparisons with the COST 2100 model cannot be made as the latter was only parametrized in indoor scenarios around 3.5 GHz or in outdoor scenarios in the VHF band.

*3) Cluster Spread Cross-Correlations:* The obtained cross-correlation coefficients are listed in Table V. The correlation between azimuth-spreads is quite strong, whereas the correlation between CAS and CDS is relatively low and could be neglected.

TABLE V. CROSS-CORRELATIONS BETWEEN CLUSTER-SPREADS

| | **<$CAS_{BS}$, $CAS_{MS}$>** | **<CDS, $CAS_{BS}$>** | **<CDS, $CAS_{MS}$>** |
|---|---|---|---|
| **Parking** | 0.9 | 0.3 | 0.4 |
| ***SB* - LOS** | 0.6 | 0.2 | 0.1 |
| ***SB* - NLOS** | 0.7 | 0.2 | 0.1 |

*4) Cluster Polarization Properties:* For each extracted multipath, cross-polar discrimination (XPD) and co-polar ratio (CPR, i.e. the ratio between both co-polar powers) are extracted. Average XPD values around 8.5 dB and 10 dB have been extracted for both vertical and horizontal polarizations, whereas the CPR is about 1.5 dB on average. These values are similar to those obtained in the WINNER and COST models.

*5) Cluster Tracking and Lifetime:* An automatic tracking algorithm [8] has been applied to track clusters over time and establish the average lifetime of clusters. The results are highlighted in Fig. 6 for a short segment of the parking route: the vertical axis is the Cluster Identification (CID), so that horizontal lines represent the lifetime in measurement snapshots.

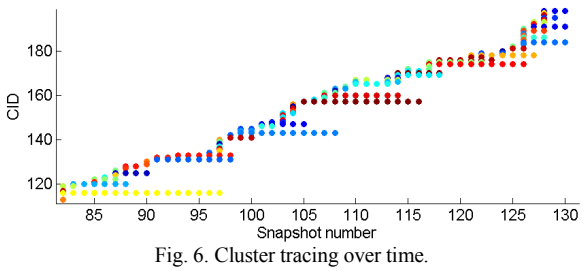



Fig. 6. Cluster tracing over time.

Resulting lifetimes range from 1 to approximately 70 snapshots, i.e. up to 1.8 meters along the trajectory.

### C. Joint Specular-Dense Cluster Parameterization

Finally, a joint specular-dense multipath clustering was performed, similarly to the COST 2100 modeling approach [3], which extends all specular clusters by a DMC cluster. Before running a modified KPM algorithm, the directional impulse response of DMC must be obtained. This is done via a beamformer [9] using a Chebyshev window with a resolution of 2.5 ns in delay and 2 degrees in angle.

When this extraction is carried out, a joint clustering algorithm is used, similarly to [9]. Taking into account both specular and DMC clusters, the cluster-spreads can be re-estimated: the resulting spreads are outlined in Table VI.

TABLE VI. MEAN (STD) OF CLUSTER SPREADS

| | **CDS [ns]** | **CAS at BS [deg.]** | **CAS at MS [deg.]** |
|---|---|---|---|
| **Parking** | 11.1 (3.8) | 12.4 (1.7) | 20.8 (1.6) |
| ***SB* - NLOS** | 14.4 (3.5) | 15.7 (3.4) | 20.2 (2.2) |

While cluster-delay spread values are only marginally improved when adding dense components, the CAS values are getting much closer to the values of WINNER and 3GPP models. This illustrates the significant of dense multipath components on the directional spreading of the energy.

## V. CONCLUSIONS

An experimental campaign conducted in suburban microcell environment has been analyzed to characterize large-scale parameters of the double-directional wireless channel in the sub-6 GHz band, and parameterize a geometry-based model using clusters in suburban areas. The main conclusions are as follows.

- This work provides an input to the parameterization of the COST 2100 channel model for urban areas, for which parameters are still missing.
- In terms of large-scale parameters, azimuth-spreads at the base station appear to be much higher (up to 24 degrees) than in 3GPP and WINNER models, although our values are vezry close to more recent models, such as QuaDRiGa.
- The cluster parameterization must be carried out jointly for specular and dense multipath clusters, as the dense multipath power can represent a large part of the received power. Cluster spreads including dense multipaths are consistent with existing models.
- The polarization properties of multipath clusters are in line with those already observed in similar environments, with cross-polar discriminations of about 8 to 10 dB.

## ACKNOWLEDGMENTS

This work was partially funded by the Interuniversity Attraction Poles Programme 7/23 BESTCOM initiated by the Belgian Science Policy Office. It was also carried out in the framework of COST Action CA15014 IRACON.

## REFERENCES

[1] P. Kyösti, et al., *IST-4-027756 WINNER II D1.1.2 v.1.1: WINNER II channel models*, Tech. Rep., 2007. [Online]. Available: http://www.ist-winner.org

[2] L. Correia, Ed., *Mobile Broadband Multimedia Networks*. New York, USA: Elsevier, 2006 – Ch. 6.8: The COST 273 MIMO channel model, pp. 364-383.

[3] L. Liu et al., "*The COST 2100 MIMO channel model*," *IEEE Wireless Communications Magazine*, 19(6), pp. 92-99, December 2012.

[4] S. Jaeckel, et al., "QuaDRiGa: a 3-D multi-cell channel model with time evolution for enabling virtual field trials," *IEEE Trans. Ant. Propagat.*, 62(6), pp. 3242-3256, 2014.

[5] A. Algans, et al., Experimental analysis of the joint statistical properties of azimuth spread, delay spread, and shadow fading," *IEEE Journal on Selected Areas in Communications*, 20(3), pp. 523-531, 2002.

[6] M. Pettersen, et al., "Characterisation of the directional wideband radio channel in urban and suburban areas," in *Proc. 50th Vehicular Technology Conference Fall*, pp. 1454-1459, 1999.

[7] N. Czink, et al., "Cluster characteristics in a MIMO indoor propagation environment," *IEEE Trans. on Wireless Comm.*, 6(4), pp. 1465-1475, 2007.

[8] N. Czink, et al., "A novel automatic cluster tracking algorithm," in *Proc. IEEE 17th International Symposium on Personal, Indoor and Mobile Radio Communications*, 2006.

[9] F. Quitin, et al., "Model parametrization and validation for specular-diffuse clustered channel models," *IEEE Trans. Ant. Propagat.*, 60(8), pp. 4019-4022, 2012.